

Intra-shell states of doubly excited atoms: diagonalization within a basis of symmetrically excited electrons

Klaus Richter and Dieter Wintgen

Fakultät für Physik, Hermann-Herder-Strasse 3, 79104 Freiburg, Federal Republic of Germany

Received 12 May 1993

Abstract. We calculate $1S^e$ intra-shell wavefunctions of highly doubly excited two-electron atoms by diagonalizing the corresponding Hamiltonian in a Sturmian-type basis set representing symmetrically excited electrons. We take into account couplings between different intra-shell manifolds. The Z -dependence of the energies of all intra-shell states up to principal quantum numbers $N = n = 12$ is examined. We investigate the nodal structure of the wavefunctions in the manifold $N = 8$ for nuclear charges $Z = 2$ and $Z = 10$ to examine the validity of the Herrick classification scheme. It turns out that this scheme appropriately describes the structure of the lower states in the multiplets but it breaks down for the higher lying states. A comparison with wavefunctions from large-scale calculations reveals that the intra-shell diagonalization overestimates the radial independent-electron character of the wavefunctions. A semiclassical interpretation of the wavefunctions is given in terms of fundamental modes of the electron-pair motion.

1. Introduction

Since the identification of doubly excited states of helium (Madden and Codling 1963) different classification schemes have been proposed for an appropriate description of these states (Cooper *et al* 1963, Macek 1968, Conneely and Lipsky 1978, Herrick 1983, Fano 1983, Lin 1984, Feagin and Briggs 1986, 1988, Macias and Riera 1991). Among the doubly excited resonant states the so-called *intra-shell* states composed of symmetrically excited electrons have retained particular interest. These states correspond to configurations with individual principal quantum numbers $N = n$ (in an independent-particle model), see e.g. Herrick (1983), Fano (1983), Lin (1984), Macias and Riera (1991), Herrick *et al* (1980), Dmitrieva and Plindov (1988), Rost *et al* (1991a, b). It has been supposed that they exhibit considerable electronic correlation since the electrons occupy similar independent-particle shells, $\langle r_1 \rangle \approx \langle r_2 \rangle$. Additional interest stems from the (still unsolved) question of whether there exists a connection between features of intra-shell states in the limit $N = n \rightarrow \infty$ and the correlation which governs the threshold behaviour of two escaping electrons in the processes of double photoionization of helium or electron-impact ionization of hydrogen (Wannier 1953, Macek and Feagin 1985).

The most frequently applied classification scheme of doubly excited states has been suggested by Wulfman (1973) and Herrick and Sinanoglu (1975) proceeding from a group theoretical analysis. It was re-interpreted by Lin (1984) in the framework of the hyperspherical adiabatic approach. Briggs and co-workers (Feagin and Briggs 1986, 1988, Rost *et al* 1991a, b) identified a relation to approximate symmetries obtained within a molecular orbital treatment of doubly excited states. Herrick (1983) and co-workers suggested a certain coupling of different individual electronic angular momenta for fixed

principal quantum numbers (N, n) to construct *doubly excited symmetry basis* (DESB) wavefunctions. They introduced two quantum numbers K, T to characterize the DESB functions. The DESB functions were assumed to approximately diagonalize the electron-electron interaction within the degenerate hydrogenic manifolds of fixed principal quantum numbers N, n . Following this classification scheme doubly excited states are labelled in terms of the set of approximate quantum numbers $N(K, T)n$ in addition to the fully conserved quantum numbers L, S, π .

Herrick and Sinanoglu (1975) concluded that low-lying DESB functions are in good agreement with CI wavefunctions which incorporate inter-shell couplings between subspaces of fixed N but varying n . On the other hand Lin and Macek (1984) performed a critical comparison between DESB states and full CI functions for $N = n = 3$ for helium. They found that DESB functions insufficiently account for radial correlations, particularly states of high bending vibration where the electrons are no longer located predominantly on different sides of the nucleus.

In his treatment Herrick made use of essentially two approximations. (i) He performed the diagonalization within each degenerate manifold of states with fixed principal quantum numbers N, n . (ii) The DESB functions do not diagonalize the electron-electron interaction but merely approximately its quadratic inverse. In the present work we calculate resonance energies and wavefunctions for symmetrically excited electrons by extending Herrick's method through diagonalization of the *entire* two-electron Hamiltonian using a basis set of (in principle) *all* states with $N = n$, i.e. we take into account couplings between different intra-shell manifolds. The states under consideration belong to an energy regime where different intra-shell manifolds overlap for the case of helium. We study highly excited states ($N = n = 8$) in order to investigate the rearrangement of nodal patterns for the different states within a given N -manifold. Examination of nodal structures of wavefunctions have been performed only for low doubly excited states (Herrick and Sinanoglu 1975, Lin and Macek 1984, Rost *et al* 1991a, b). We find that the radial part of low-lying states in each intra-shell manifold seems to separate approximately in independent particle coordinates. The corresponding nearly rectangular nodal pattern (with respect to the electron distances r_1, r_2) rearranges to a diagonal pattern for the states with the highest bending excitation of the electrons.

Herrick's K, T classification is frequently used in the literature to label intra-shell states of two-electron atoms. One aim of this paper is to investigate how far the approximate separability of the wavefunctions, i.e. the conservation of the quantum number K , remains valid for the higher lying states of each manifold ($T \equiv 0$ for $^1S^e$ states considered here).

We compare results of the diagonalization of the full Hamiltonian within a basis set of symmetrically excited electrons with the resulting energies and wavefunctions from calculations using near-complete basis sets.

Finally we will show that the nodal structure of specific classes of wavefunctions can be understood in terms of fundamental classical periodic motion of the electron pair. Such a description is particularly suitable for wavefunctions which cannot be characterized by global approximate quantum numbers but which approximately separate in local coordinates along and perpendicular to the corresponding classical periodic orbits (Gutzwiller 1990).

2. Methods of calculation

2.1. Diagonalization techniques

The non-relativistic Hamiltonian of a two-electron atom (or ion) with nuclear charge Z reads (atomic units are used throughout the paper)

$$H = \frac{p_1^2}{2} + \frac{p_2^2}{2} - \frac{1}{r_1} - \frac{1}{r_2} + \frac{1/Z}{r_{12}} = E \tag{1}$$

where E is the Z -scaled energy ($E \rightarrow E/Z^2$), r_1, r_2 are the Z -scaled ($r_i \rightarrow Zr_i$) electron-nucleus distances, and r_{12} denotes the Z -scaled distance between the electrons. In the present paper we compare energy positions and wavefunctions obtained from the diagonalization of the Hamiltonian (1) within a basis set of equally excited electrons with converged results from *ab initio* calculations using a truncated but new-complete basis set.

For both diagonalization procedures we use a transformation of the Schrödinger equation into perimetric coordinates (James and Coolidge 1937, Pekeris 1958, Richter *et al* 1992) which are defined as

$$x = r_1 + r_2 - r_{12} \quad y = r_1 - r_2 + r_{12} \quad z = -r_1 + r_2 + r_{12} \quad x, y, z \geq 0. \tag{2}$$

For total angular momentum $L = 0$ the Hamiltonian (1) transforms to

$$H = \frac{1}{(x+y)(x+z)(y+z)} \sum_{i,j=1}^3 \frac{\partial}{\partial q_i} P_{ij}^{(3)}(x, y, z) \frac{\partial}{\partial q_j} - \frac{2}{x+y} - \frac{2}{x+z} + \frac{2/Z}{y+z} \tag{3}$$

where (q_1, q_2, q_3) are defined as (x, y, z) . The $P_{ij}^{(3)}$ are polynomials of degree 3 (see, for example, Frost *et al* 1964, Zhen 1990). Each degree of freedom is expanded in a Sturmian basis set and the product functions are symmetrized (the electron exchange corresponds to an exchange of the perimetric coordinates y and z),

$$\Phi_{nmk}(x, y, z) = \phi_n(2\beta x) [\phi_m(\beta y)\phi_k(\beta z) + \phi_k(\beta y)\phi_m(\beta z)]. \tag{4}$$

The $\phi_n(u)$ are defined by

$$\phi_n(u) = L_n(u) e^{-u/2} \tag{5}$$

and $L_n(u)$ are the Laguerre polynomials. One advantage of using perimetric coordinates in combination with a Sturmian basis is that the volume element

$$dV = \frac{1}{32}(x+y)(x+z)(y+z) dx dy dz \tag{6}$$

cancels the singularities in the kinetic energy and in the potential terms if matrix elements are calculated. All matrix elements are of simple analytic form. Their calculation requires only integer arithmetic and is fast and accurate. In addition, selection rules guarantee that most of them vanish. The resulting matrix equation is of banded, sparse structure and allows for efficient diagonalization.

The Schrödinger equation is now transformed into a matrix equation of the particular form

$$(\beta^2 \hat{T} + \beta \hat{V} - E \hat{N}) \Psi = 0. \tag{7}$$

The scaled matrices $\hat{T}, \hat{V}, \hat{N}$ of the kinetic energy, potential, and the unit operator do not depend on β .

Starting from equation (7) we use the method of complex rotation (Reinhardt 1982, Ho 1983) to calculate accurate *ab initio* energy positions as reference values for a comparison

with the approximate intra-shell diagonalization discussed below. The complex scaling leads to a complex symmetric eigenvalue problem, since the scale parameter β becomes complex-valued. However, the matrices $\hat{\mathbf{T}}$, $\hat{\mathbf{V}}$, $\hat{\mathbf{N}}$ are still real symmetric. We use basis functions with a total nodal-number $\mathcal{N} = n + k + m$ (see equation (4)) up to 50 which corresponds to matrix dimensions up to 12051. More details about the numerical solution of the complex matrix equation (6) and the different convergence checks we performed can be found in (Richter *et al* 1992, Bürgers and Wintgen 1993).

In addition to our *ab initio* method we use the following procedure (which we call *intra-shell diagonalization*) to obtain energies based on a reduced basis set of symmetrically excited electrons.

(i) We start from the rearranged matrix equation (6)

$$\left(\hat{\mathbf{T}} - \frac{E}{\beta^2} \hat{\mathbf{N}}\right) \Psi = -\frac{1}{\beta} \hat{\mathbf{V}} \Psi \quad (8)$$

in the unrotated form, i.e. for real β . In solving the eigenvalue problem for β (with E/β^2 fixed) we treat the resonances as bound states. The potential matrix $\hat{\mathbf{V}}$ is composed of a part $\mathbf{V}_{\text{indep}}$ containing the electron–nuclear interactions $1/r_i$ and a part containing the inter-electron potential $\mathbf{V}_Z = 1/(Zr_{12})$. In a first step we solve the independent electron problem ($Z = \infty$), i.e. the matrix equation (8) is diagonalized to obtain the eigenfunctions $\Psi_{N,n}$ with energies $E = -1/(2N^2) - 1/(2n^2)$.

(ii) In a second step the basis functions $\Psi_{N=n}$ of symmetrically excited electrons ($N = n$) with energy $E_N = -1/N^2$ are isolated. Each eigenvalue E_N is N times degenerated. Note that with the choice $E/\beta^2 = -1$ the eigenfunctions are represented *exactly* as a finite sum over the Sturmian basis functions with total nodal-number $n + k + m \leq 2N$.

(iii) In a third step (which may be omitted) the inter-electron potential is pre-diagonalized within each $N \times N$ intra-shell block of degenerate states, which accounts for first-order degenerate perturbation theory. The symmetry breaking electron–electron interaction removes the degeneracy, and the perturbative treatment yields the correct $1/Z \rightarrow 0$ limit of the wavefunctions of the full Hamiltonian.

(iv) In the last (fundamental) step the full Hamiltonian is diagonalized in the intra-shell basis set $\{\Psi_{N=n}\}$ of all N by solving the generalized eigenvalue problem (8) with E/β^2 fixed to -1 to obtain eigenvalues $-1/\beta$ and the corresponding energies $E = -\beta^2$.

There is a sophisticated reason, why we use the unusual arrangement (8) of the Schrödinger equation. In general Sturmian basis functions are used to solve the Schrödinger eigenvalue problem with a fixed scale parameter β for the entire basis set. β is chosen to give the approximate fall-off behaviour of the wavefunctions in the particular energy range of interest, i.e. $\beta \approx 1/N$. In solving the eigenvalue problem (8) we exploit a scaling property with respect to β and do not fix β but $E/\beta^2 \equiv -1$. Each diagonalization now yields eigenvalues $-1/\beta$, i.e. each eigenstate has its own Sturmian parameter. This procedure has the advantage that the scale parameter β of the basis functions is automatically adjusted to a suitable value over a large range in energy. All the basis functions possess the exact fall-off behaviour in the independent-electron limit $Z \rightarrow \infty$. This procedure combines the advantages of a complete basis set (the Sturmian functions represent bound and continuum states) with efficient diagonalization techniques to obtain well converged eigenstates within a wide range of energies.

The steps (i)–(iii) must be performed only once. Only the diagonalization (iv), which in the following we will refer to as *intra-shell diagonalization*, depends explicitly on the nuclear charge Z . The intra-shell diagonalization contains two approximations: the use

of a (truncated) L^2 -basis set to describe resonance positions and—more importantly—the constraint to a basis set of symmetrically excited electrons.

For the present calculations we included all independent particle intra-shell basis states up to quantum numbers $N = n = 14$, i.e. 105 basis functions. The corresponding set containing all intra- and inter-shell Sturmian basis functions would consist of 1925 states.

2.2. Relation to Herrick's approach

There are several differences between the present intra-shell diagonalization and the group theoretical approach of Herrick (1983) and co-workers. The DESB functions constructed by Herrick are certain linear combinations of *bound* state hydrogenic wavefunctions for the individual electrons with fixed principal quantum numbers $N = n$ (i.e. they do not represent a complete basis set even if inter-shell states with $N \neq n$ were included). In addition, mixing between different intra-shell manifolds is neglected, i.e. N, n are assumed to be good quantum numbers. The DESB functions are constructed to diagonalize the operator $B^2 = (\mathbf{b}_1 - \mathbf{b}_2)^2$, where \mathbf{b}_i are the individual electronic Runge–Lenz vectors. Taking into account the so-called Pauli replacement (within a fixed electronic shell N)

$$\mathbf{r}_i = \frac{3N}{2Z} \mathbf{b}_i \quad \text{i.e. } \mathbf{B} = \frac{2Z}{3N} (\mathbf{r}_1 - \mathbf{r}_2) \quad (9)$$

the DESB functions approximately diagonalize the operator of the quadratic inverse of the inter-electron interaction within a fixed $N = n$ manifold. Therefore the DESB approach can be considered as an approximate first order perturbative treatment of the operator $1/(Z|\mathbf{r}_1 - \mathbf{r}_2|)$. In comparison to the present intra-shell diagonalization (step (iv)) the DESB approach thus makes use of two additional approximations: neither the whole two-electron Hamiltonian is diagonalized nor are couplings between different intra-shell manifolds taken into account.

2.3. Classification

In order to assign quantum numbers to the calculated states we will use Herrick's classification scheme. Besides the principal quantum numbers N, n , new quantum numbers K, T are introduced which replace the individual electron angular momenta l_1, l_2 . T ($T = 0$ for S states) is the body-fixed azimuthal quantum number $T = \mathbf{L} \cdot \mathbf{B}$ with the body-fixed z -axis directed along the inter-electron distance $\mathbf{r}_1 - \mathbf{r}_2$. The label K counts the eigenvalues of B^2 and describes the angular correlation of the electrons. For symmetrically excited electrons Herrick and co-workers derived an approximate formula for the average value Θ_{12} of the angle between the electron radius vectors $\mathbf{r}_1, \mathbf{r}_2$ as function of N, K, T (Herrick *et al* 1980) (given here for $L = T = 0$),

$$\langle \cos \Theta_{12} \rangle = \frac{4N^2 - 3(N + K)^2 - 1}{8N^2}. \quad (10)$$

For S states K takes the values $K = N - 1, N - 3, \dots, -(N - 1)$. A positive value of K corresponds to a dominant localization of the electrons on opposite sides of the nucleus. Thus decreasing values of K label states of increasing electron repulsion. On the other hand, negative values of K belong to states of high bending vibrations of the electrons. In these states the electrons are located to a large extent on the same side of the ionic core. In the limit of large N the correlation angles (10) have a range of values $60^\circ \leq \Theta_{12} \leq 180^\circ$. This behaviour for symmetrically excited electrons is in striking contrast to correlation

angles derived from a dipole-channel treatment for inter-shell states ($N, n \gg N$), where $-K$ has the meaning of the electric (Stark) quantum number for the inner electron N and $\langle \cos \Theta_{12} \rangle \sim -K/N$ ranges from $0^\circ < \Theta_{12} < 180^\circ$.

Herrick's classification is equivalent to labelling schemes originating from different approaches as documented in the literature: Lin (1984) proposed the (K, T) -classification scheme resulting from an empirical analysis of adiabatic hyperspherical potential curves and wavefunctions. A derivation of Herrick's quantum numbers within the molecular framework was given by Briggs and coworkers (Feagin and Briggs 1986, 1988, Rost *et al* (1991a, b)). The whole set of (exact and approximate) quantum numbers finally leads to the classification $N(K, T)n^{2S+1}L^\pi$. Since we will deal exclusively with $1S^e$ intra-shell states ($S = 0, L = T = 0, \pi$ even) we will use the simplified classification (N, K) in the following.

3. Results

We will report our results for the energies and expectation values first and then examine the structure of the corresponding wavefunctions. Finally, we discuss the validity of the classification scheme for highly doubly excited states.

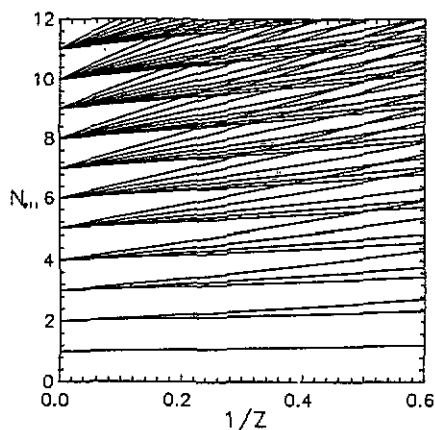


Figure 1. Plot of the effective quantum number $N_{\text{eff}} = 1/\sqrt{-E}$ of $1S^e$ intra-shell states plotted against $1/Z$. The energies are obtained by using the reduced basis set of symmetrically excited electrons.

3.1. Energies and expectation values

In figure 1 we plot the effective quantum number $N_{\text{eff}} = 1/\sqrt{-E}$ as a function of $1/Z$ to get an idea of the global structure of the intra-shell spectrum. The Z -correlation diagram is plotted for integer as well as non-integer values of Z to get insight into the systematics of the Z -dependence. At the independent particle limit ($1/Z = 0$) all levels within an $(N = n)$ intra-shell manifold are N times degenerated. Figure 1 depicts the level splittings with increasing perturbation $1/(Zr_{12})$. The lowest levels of each manifold, $K = N - 1$, correspond to electron pairs in a near-collinear arrangement $\Theta_{12} \approx \pi$, i.e. these are states of minimal inter-electron repulsion. Higher lying levels with increasing off-collinear parts of

Table 1. Energies and expectation values ($\cos \Theta_{12}$) of $1S^e$ intra-shell states in helium. Results from the intra-shell diagonalization (column 3, 5) are compared with results from *ab initio* calculations (compl. rot.). The states are labelled by $N = n, K$ in the classification scheme of Herrick. The last column contains analytical values from formula (10). A dash indicates that the state is below the $(N - 1)$ -threshold.

N	K	-Energies (au)		- $\langle \cos \Theta_{12} \rangle$ ($Z = 2$)		- $\langle \cos \Theta_{12} \rangle$ ($Z = 10$)	
		Intra-shell	Compl. rot.	Intra-shell	Compl. rot.	Intra-shell	Eqn (10)
1	0	2.8708	2.9037	0.054	0.064	0.011	0.000
2	1	0.7711	0.7779	0.379	0.448	0.366	0.375
2	-1	0.5979	0.6219	-0.224	-0.291	-0.337	-0.375
3	2	0.3519	0.3535	0.545	0.601	0.536	0.556
3	0	0.3041	0.3175	-0.066	-0.033	-0.081	-0.111
3	-2	0.2425	0.2574	-0.214	-0.351	-0.407	-0.444
4	3	0.2003	0.2010	0.643	0.690	0.635	0.656
4	1	0.1826	0.1878	0.106	0.200	0.091	0.093
4	-1	0.1560	0.1683	-0.207	-0.110	-0.216	-0.281
4	-3	0.1299	0.1411	-0.168	-0.534	-0.442	-0.469
5	4	0.1291	0.1294	0.706	—	0.700	0.720
5	2	0.1207	0.1233	0.233	0.329	0.222	0.240
5	0	0.1089	0.1153	-0.083	0.028	-0.092	-0.120
5	-2	0.0930	0.1024	-0.256	-0.199	-0.277	-0.360
5	-4	0.0809	0.0896	-0.120	-0.712	-0.466	-0.480
6	5	0.0901	0.0901	0.751	—	0.746	0.764
6	3	0.0855	0.0863	0.333	—	0.321	0.347
6	1	0.0794	0.0821	0.026	—	0.020	-0.014
6	-1	0.0710	0.0772	-0.193	-0.060	-0.186	-0.236
6	-3	0.0614	0.0679	-0.243	-0.152	-0.310	-0.403
6	-5	0.0553	0.0621	-0.098	-0.747	-0.483	-0.486
7	6	0.0664	0.0664	0.784	—	0.780	0.796
7	4	0.0636	0.0640	0.411	—	0.400	0.429
7	2	0.0600	0.0606	0.117	—	0.113	0.122
7	0	0.0555	0.0582	-0.081	—	-0.094	-0.122
7	-2	0.0495	0.0500	-0.262	-0.167	-0.242	-0.306
7	-4	0.0434	0.0469	-0.207	-0.346	-0.333	-0.429
7	-6	0.0403	0.0455	-0.067	-0.776	-0.494	-0.490
8	7	0.0509	0.0508	0.810	—	0.806	0.820
8	5	0.0491	0.0497	0.473	—	0.462	0.492
8	3	0.0469	0.0481	0.205	—	0.193	0.211
8	1	0.0441	0.0463	-0.014	—	-0.013	-0.023
8	-1	0.0405	0.0441	-0.172	—	-0.166	-0.211
8	-3	0.0362	0.0405	-0.264	-0.204	-0.280	-0.352
8	-5	0.0324	0.0366	-0.163	-0.195	-0.349	-0.445
8	-7	0.0307	0.0348	-0.132	-0.802	-0.502	-0.492

the two-electron wavefunction belong to states of successively increasing bending excitation. For small N or large Z different N -manifolds are energetically well separated and first order degenerate perturbation theory, i.e. diagonalization of $1/(Zr_{12})$ in the subspace of degenerated states, may be well justified (Herrick *et al* 1980, Dmitrieva and Plindov 1988) However, for helium ($1/Z = 0.5$) intra-shell manifolds with $N > 4$ intersect, even though avoided crossings between levels of different N are only small (they are actually invisible on the figure). Nevertheless, beyond the region of isolated N -manifolds mixing between different N states occurs and the validity of approaches which ignore inter-shell couplings

(for example Herrick's DESB ansatz) has to be examined.

The lowest states ($K = N - 1$) of each N -multiplet exhibit only a weak Z -dependence. The classical phase space regions to which these states belong are only negligibly affected by varying Z . This is not the case, however, for states of high bending vibration. The classical allowed region of the electron-pair motion is strongly affected by changing Z , resulting in a considerable (non-trivial) Z -dependence of the energies and wavefunctions of the highest states with $K = -(N - 1)$.

In table 1 we list resonance positions and expectation values of $\cos \Theta_{12}$ for intra-shell states up to $N = 8$. Results from the diagonalization within the basis set of symmetrical electrons are compared with energy values obtained from *ab initio* calculations described in the previous section. In columns 5 to 8 expectation values of $\cos \Theta_{12}$ are given for $Z = 2$ (calculated by intra-shell diagonalization and *ab initio*), for $Z = 10$ (from intra-shell diagonalization), and from the group theoretical analytical formula (10). With increasing excitation N the values of $\langle \cos \Theta_{12} \rangle$ for maximal $K = N - 1$ reflect the increasing alignment of the electrons along the body-fixed z -axis $\Theta_{12} = \pi$. Within each intra-shell manifold N higher vibrational states (lower K) reduce the polarization of the electrons. For helium the values $\langle \cos \Theta_{12} \rangle$ from the intra-shell diagonalization are generally smaller than the *ab initio* results, since the reduced Hilbert space of symmetrical basis-set configurations does not allow for the high degree of polarization as in the full calculations. Herrick's analytical formula (10) predicts values for the correlation angle between $-1 \leq \cos \Theta \leq 0.5$, i.e. ($180^\circ \geq \Theta_{12} \geq 60^\circ$). The analytical values are in reasonable agreement with the numerical results for $Z = 10$. Since the ($N = 8$)-multiplet is energetically separated (see figure 1), mixing between different intra-shell manifolds turns out to be of minor significance. For helium, equation (10) reproduces the numerical results only for the lowest states of each N -manifold. The highest states show a non-monotonic behaviour in the expectation values of the correlation angle. The analytical limiting value $\Theta = 60^\circ$ is not reached, which indicates strong inter-shell mixings in the *ab initio* states of low K . (Mixing coefficients are given in table 2 and will be discussed in section 3.2.

Table 2. Weights of pre-diagonalized basis states for the ($N = 8$) eigenfunctions from the intra-shell diagonalization for helium. Only the weights for states (N, v) of similar character are listed. The label $v = (N - K - 1)/2$ denotes the number of nodal bending excitations.

K	v	(6, v)	(7, $v - 1$)	(7, v)	(8, v)	(9, v)	(9, $v + 1$)	(10, v)
7	0	0.012	—	0.123	0.982	-0.142	0.029	0.004
5	1	0.005	0.029	0.116	0.981	0.136	0.065	0.009
3	2	0.002	0.066	-0.080	-0.977	0.112	0.116	0.018
1	3	-0.003	-0.127	0.003	-0.946	-0.048	0.195	0.025
-1	4	0.062	-0.243	0.112	-0.845	-0.086	-0.289	0.033
-3	5	0.074	0.362	-0.004	0.486	-0.309	-0.310	0.080
-5	6	—	0.262	-0.201	0.086	0.177	0.441	0.169
-7	7	—	0.115	—	-0.187	-0.327	0.338	-0.012

A comparison of the energies obtained within the intra-shell basis set and a complete basis set shows considerable agreement for states of strong polarization along the axis $\Theta_{12} = \pi$ with (absolute) errors ranging up to 1%. The inaccuracy of the intra-shell diagonalization increases with decreasing K and is largest for the highest states of each N -manifold. Again this indicates that contributions from basis states of asymmetrically excited electrons, which are not taken into account in the intra-shell diagonalization, are of particular importance for the states of high bending excitation.

3.2. Nodal structure and classification of the wavefunctions

In this section we study the nodal structures of symmetrically doubly excited states. We will particularly focus on the rearrangement of the wavefunctions for different K but N fixed. As representative manifold we chose $N = 8$. For helium, the corresponding energy range already belongs to the N -mixing regime but it is still feasible to obtain fully converged results within the different approaches. In addition, the number of nodal excitations is large enough to study the rearrangement of nodal patterns in the multiplet. Before we examine plots of the wavefunctions we will first study the contributions of pre-diagonalized (PD) basis states $\Psi_{N,K}^{(PD)}$ (obtained from step (iii) as described in section 2.1) to the eigenstates $\Psi_{N,K}$ of the intra-shell diagonalization (step (iv)).

3.2.1. *Mixing coefficients for ($N = 8$) states of helium.* The weights w_{nk}^{NK} of the eigenstate decomposition

$$\Psi_{N,K} = \sum_n \sum_{k=-l(n-1)}^{n-1} w_{nk}^{NK} \Psi_{n,k}^{(PD)} \quad (11)$$

yield information about the degree of mixing between states of different K and of different N -shells. For simplicity, we list in table 2 the dominant weights of the ($N = 8$)-eigenstates only. Contributions of other basis states which in some cases are of considerable magnitude are not given in table 2.

In addition to K , we introduced the label $v = (N - K - 1)/2$ —originally used by Herrick (1983)—to count the number of bending excitations in Θ_{12} . Table 2 shows that the states of low bending excitation ($v = 0, 1, 2$) are nearly identical with the corresponding pre-diagonalized basis states. They are fairly well described within the first order perturbative approach. On the contrary, the states of high bending excitation ($v = 5, 6, 7$) exhibit strong mixings between states of different N -shells and their character can no longer be described by a dominant contribution of some pre-diagonalized state $\Psi_{NK}^{(PD)}$. We recall that the weights tabulated are derived from the intra-shell diagonalization omitting basis states of asymmetrical-electron character. Their inclusion will certainly not decrease (but presumably increase) the strong inter- N mixing. The occurrence of strong mixings questions the interpretation and validity of Herrick's quantum number K for the uppermost states of each N -manifold. It may still be used as a label but the *character* of the high v states of helium certainly differs from the pre-diagonalized states giving the large Z -limit.

3.2.2. *Probability densities for the ($N = 8$) states in helium.* In the following we will examine the nodal structures of the ($N = 8$) wavefunctions in helium derived from the intra-shell diagonalization as a further check of the validity of the large Z -limit classification. Comparisons with wavefunctions derived for the nuclear charge $Z = 10$ allow us to study the transition from the perturbative to the N -mixing regime. In addition, we compare our results with full quantum calculations for helium.

The wavefunctions depend on three degrees of freedom r_1, r_2, Θ_{12} . We plot the probability density of each wavefunction in three different symmetry planes of configuration space. The three planes are defined by (i) $\Theta_{12} = \pi$, i.e. the collinear configuration with both electrons on different sides, (ii) $\Theta_{12} = 0$, i.e. the collinear configuration with both electrons on the same side, and (iii) $r_1 = r_2$, i.e. the so-called Wannier configuration. The configurations are drawn schematically on top of figure 2. For helium, figure 2 depicts the probability distributions of all ($N = 8$) intra-shell states. In the first and second column

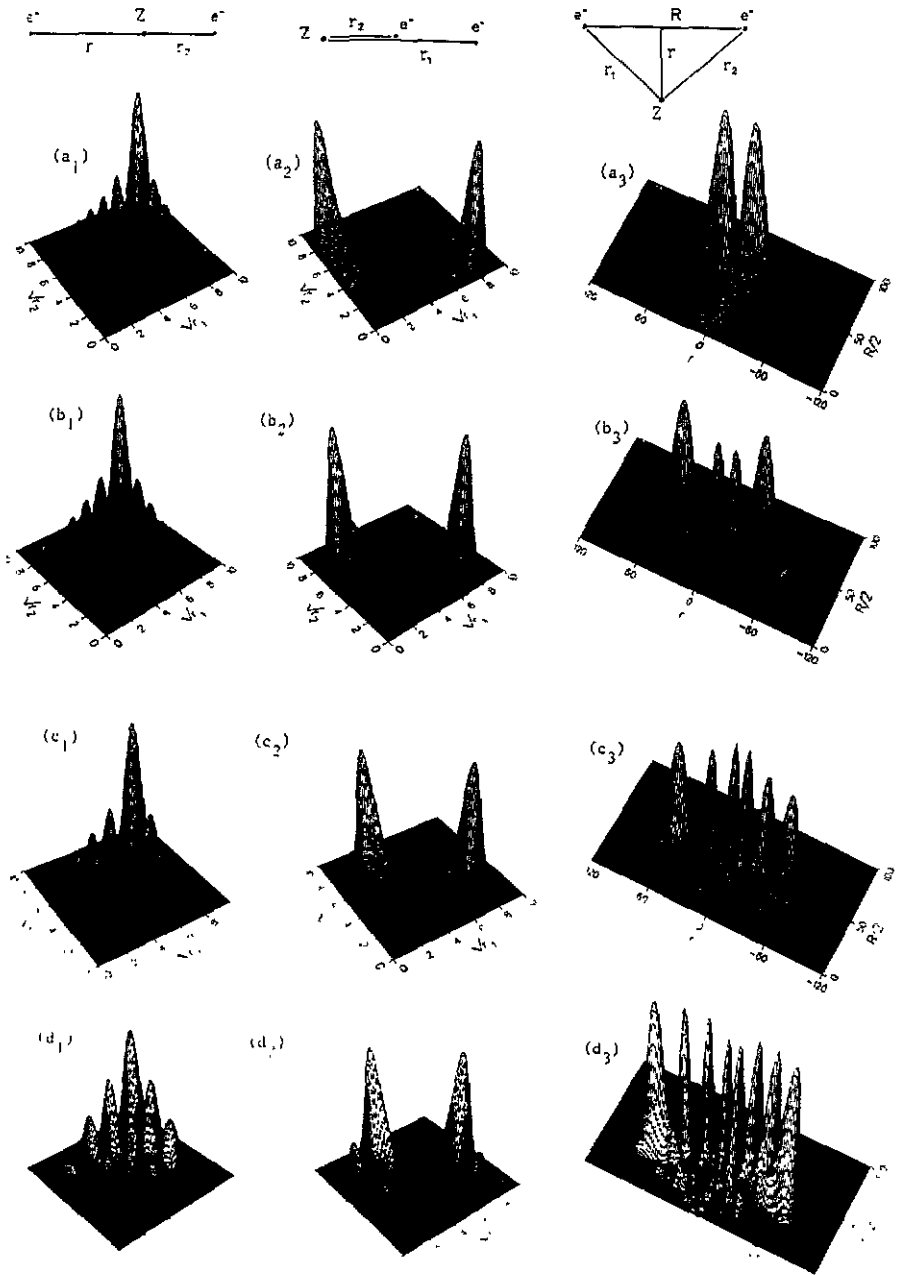


Figure 2. Conditional probability densities of all helium intra-shell states for $N = n = 8$ calculated by intra-shell diagonalization. The densities are plotted for fixed angle $\Theta_{12} = \pi$ (first column), $\Theta_{12} = 0$ (second column) and for $r_1 = r_2$ (third column), respectively. On top of the figure the electron configurations of the different symmetry planes are displayed schematically. Probability distributions are shown for $K = 7$ down to $K = -7$ ((a) to (h)). The probability maxima in the $(\Theta_{12} = 0)$ plane are about five times smaller on the average than the maxima in the other symmetry planes. The axes in the plots of the first two columns have a quadratic scale to account for the typically quadratical spacing of nodal lines in Coulomb systems.

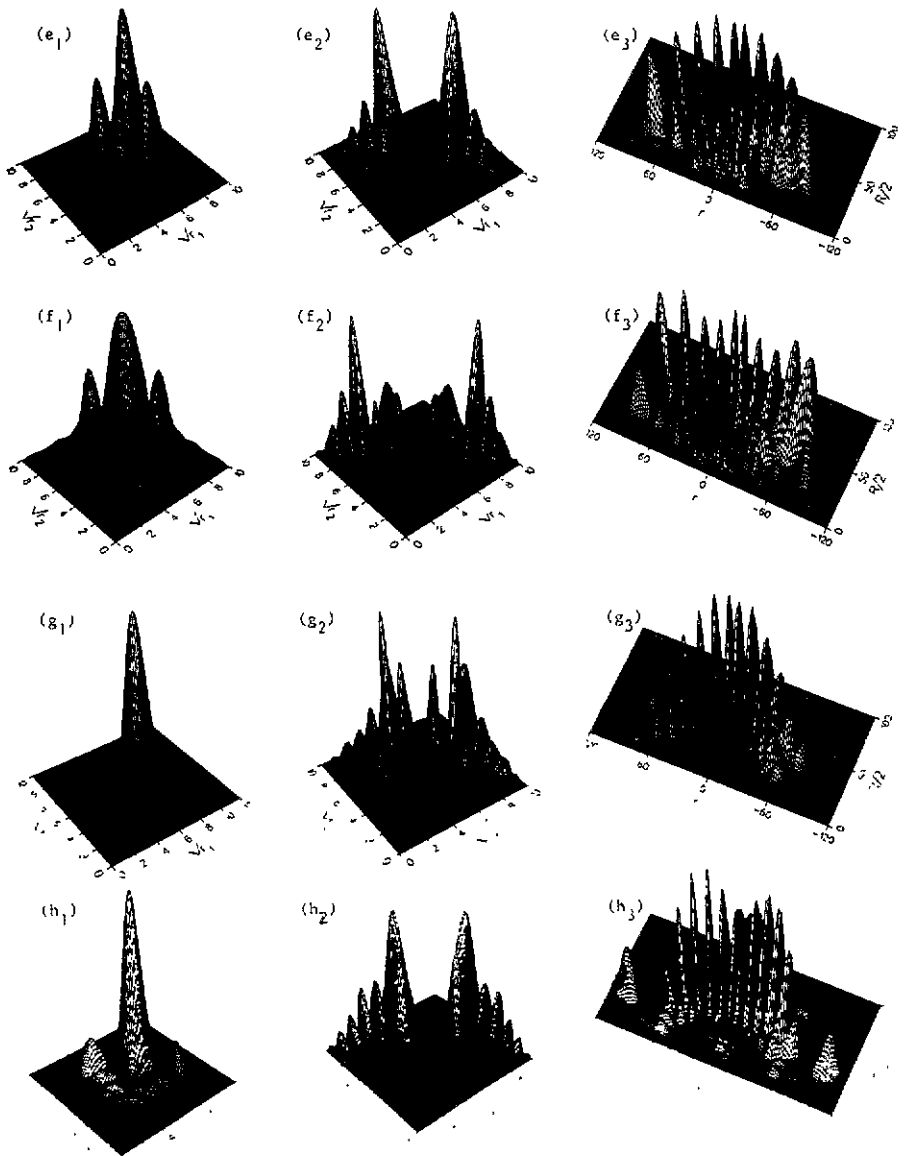


Figure 2. (Continued)

probability densities are plotted as functions of r_1, r_2 for the collinear planes $\Theta_{12} = \pi, 0$, respectively. Considering the typical quadratic spacing of nodal lines in Coulombic systems, we obtain nearly constant nodal distances by using quadratically scaled axes.

The third column of the figure contains probability densities in the Wannier plane as functions of $r = [(r_1 + r_2)/2]$ and $R = |r_1 - r_2|$. In the plots of the third column the nucleus is supposed to be at $(R, r) = (0, 0)$. The angle Θ_{12} is given in terms of R and r by $\Theta_{12} = 2 \tan^{-1}(R/(2r))$. Thus $r = 0$ denotes a collinear symmetrical arrangement of the electrons ($\Theta_{12} = \pi$) in addition to the symmetric character $r_1 = r_2$. $R = 0$ belongs to the classically forbidden configuration $r_1 = r_2, \Theta_{12} = 0$, i.e. the electrons are located at the

same place in configuration space. The third column represents the probability distributions for a single electron. The densities of the second are given by a reflection of the plot along the r -axis. Due to the multiplication of the probability densities with the volume element $R^2 r^2 dR dr$ of the (R, r) representation the densities vanish on the line $r = 0$.

The state of lowest bending excitation $(N, K) = (8, 7)$ depicted in figure 2(a) can be described as follows. In the $(\Theta_{12} = \pi)$ -plane, figure 2(a₁), the wavefunction exhibits a nearly rectangular nodal pattern with respect to the coordinates r_1, r_2 . The off-collinear part $(\Theta_{12} \neq \pi)$ of the wavefunction is visible from figure 2(a₃) since constant Θ_{12} belongs to straight lines $R/2 = r \tan(\Theta_{12}/2)$ in the r, R plane. The probability density decreases exponentially indicating a zero point motion in the bending degree of freedom. Finally, figure 2(a₂) shows the probability distribution with both electrons on the same side, i.e. $\Theta_{12} = 0$, exhibiting significant contributions only when one electron is close to the nucleus, i.e. $r_1 \approx 0$ or $r_2 \approx 0$. This indicates that only an exponentially decreasing part of each polarized electron extends to the side of the nucleus where the other electron is located. Summarizing the plots the $(N, K) = (8, 7)$ state is composed of a strongly polarized electron wavefunction aligned near the axis $\Theta_{12} = \pi$ with only a zero-point bending excitation.

The $(N = 8)$ states with decreasing $K = 5, 3, 1$ are depicted in figures 2(b)–(d). They are characterized by a successive transfer of nodal excitations from the $(\Theta_{12} = \pi)$ -plane into the bending degree of freedom, see the third column of figure 2. The number of bending excitation nodes are described by the vibrational quantum number ν as defined above.

With decreasing K the successive decrease of nodal lines in the $(\Theta_{12} = \pi)$ -plane is accompanied by a rearrangement of the nodal structure. For high K , parts (a)–(c), the wavefunctions have a checkered pattern with respect to r_1, r_2 , whereas for low K the nodal surfaces are nearly spherical, parts (f), (g). The energetically highest state, $K = -7$, part (h), shows nodal lines approximately located on diagonals in the (r_1, r_2) -plane.

The rectangular nodal pattern of the high K (low ν) states exhibits a close similarity to a product wavefunction for the radial parts of two independent electrons, i.e. the wavefunctions approximately separate in independent particle coordinates r_1, r_2 and the use of the hydrogenic principal quantum numbers N, n is justified for these states. The wavefunctions with near-spherical or diagonal nodal lines indicate a near-separation in coordinate systems using the hyper-radius $\mathcal{R} = (r_1^2 + r_2^2)^{-1/2}$ or the inter-electron distance $R = r_1 - r_2$, respectively.

The maximum probability densities of all $(N = 8)$ states in the $(\Theta_{12} = 0)$ -plane (second column in figure 2) are about five times smaller on the average than the density maxima for $\Theta_{12} = \pi$. Hence, these parts of the wavefunctions are of less importance for a classification. However, it is worth mentioning that they show a checkered nodal pattern, too. Along the symmetry line $r_1 = r_2$, $(\Theta_{12} = 0)$ the probability density is strongly suppressed.

The nodal structure in the $(r_1 = r_2)$ -plane (third column of figure 2) does not behave as regular as for the other symmetry planes. As is visible from the third column of figure 2, the probability distributions of states with moderate or high bending excitation, i.e. $K = 1, -1, -3, -7$, exhibit an irregular nodal structure. Except for the state $K = -7$ it is possible to assign a definite nodal number ν counting the minima, i.e. bending excitations, between the dominant probability peaks. However, nodal lines are in general not regular, i.e. they are not located along lines of constant angle Θ_{12} , which would appear as rays beginning at $(0, 0)$ in the plots of the third column. It is only for $K = 7, 5$ and -5 (parts (a), (b), and (g)) that such a simple pattern approximately emerges. From the nodal analysis of the wavefunctions we again conclude that the quantum numbers $N = n, K$ as derived from the large Z -limit are only of limited validity for the higher states of each multiplet in that they do not count regular nodal surfaces.

3.2.3. ($N = 8$) states from intra-shell diagonalization for $Z = 10$. As is visible from figure 1, the ($N = 8$)-multiplet is energetically well separated from neighbouring N -levels for $Z = 10$. Thus the intra-shell diagonalization is nearly equivalent to first-order perturbation theory. (The wavefunctions should then be similar to Herrick's DESB functions also.) Hence, results for $Z = 10$ can be considered as representing the perturbative limit of the two-electron problem. A comparison between $Z = 2$ and $Z = 10$ intra-shell states may therefore reveal a change in the wavefunction character due to the transition from the perturbative to the N -mixing regime.

Figure 3 depicts some ($N = 8$)-wavefunctions obtained from intra-shell diagonalization for nuclear charge $Z = 10$. As examples we choose the two energetically lowest and highest states. A comparison of the states $(N, K) = (8, 7)$ and $(8, 5)$ for $Z = 10$, figure 3(a), (b), with the corresponding states for $Z = 2$ in figure 2 shows that they are very similar in their structure. The probability distribution of the $Z = 10$ states is slightly more compact, i.e. they extend up to $r_i \approx 8$ compared to $r_i \approx 9$ for helium (note, that we use Z -scaled units).

Such a close similarity is no longer observed, however, for the highest states of the multiplet, as can be seen from a comparison of the probability distributions in the $(\Theta_{12} = \pi)$ symmetry plane (see parts (h) in figures 2 and 3). The $(\Theta_{12} = \pi)$ probability density of the state $Z = 10$, $K = -7$ exhibits no nodal excitation perpendicular to the Wannier saddle line $r_1 = r_2$. The probability distribution at $\Theta_{12} = \pi$ approximately has nodal lines at fixed hyperradius \mathcal{R} . The probability distribution on the Wannier-saddle $r_1 \equiv r_2$ characterizing maximum bending excitation appear to be not as regular structured as in the collinear symmetry planes. A more careful analysis of these wavefunction shows that even these states of high bending excitation approximately possess nodal lines at fixed values of Θ_{12} , i.e. the separation with respect to Θ_{12} is conserved for $Z = 10$ but not for helium (figure 2 (h₃)).

We finally note that the simple pattern of figure 3(g₁) does not reflect a maximum probability at the classical turning point of the symmetric stretch motion $r_1 \equiv r_2$, but a concentration of the probability near the point where the so-called Langmuir orbit (see below) passes through the $\Theta = \pi$ -plane. As can be seen from part (g₃) the motion (nodal surfaces) of the state takes place dominantly in the bending degree of freedom.

In summary, we conclude that the lowest states of each helium N -manifold are in considerable agreement with wavefunctions obtained by the perturbative large- Z limit. Herrick's classification scheme is appropriate for these states but it breaks down for the highest states of each multiplet. $N = n$ and K can still be used as labels but they lose their physical meaning in order to describe the nodal character of the helium states.

3.2.4. ($N = 8$) states using a complete basis set for helium. The wavefunctions discussed so far were obtained by diagonalizing the Hamiltonian (3) using a basis set of *all* intra-shell states up to $N = 14$, but omitting basis functions of asymmetrically excited electrons (inter-shell states). Therefore in addition to the N - and K -mixings analysed in the preceding section, mixing with inter-shell states may also influence the character of the intra-shell functions. Macias and Riera (1991) found considerable avoided crossings in Z -correlation diagrams near $Z = 2$ between low-lying doubly excited intra- and inter-shell levels, which give rise to character mixing and exchange.

To obtain rigorous results we diagonalized the Hamiltonian (3) in a near-complete basis set taking into account all basis functions with a total number of nodes up to $\mathcal{N} = n + k + m = 50$ (see equation (4)). The resulting probability distributions for the states $(N, K) = (8, 7)$ and $(8, 5)$ are displayed in figure 4. Compared with the

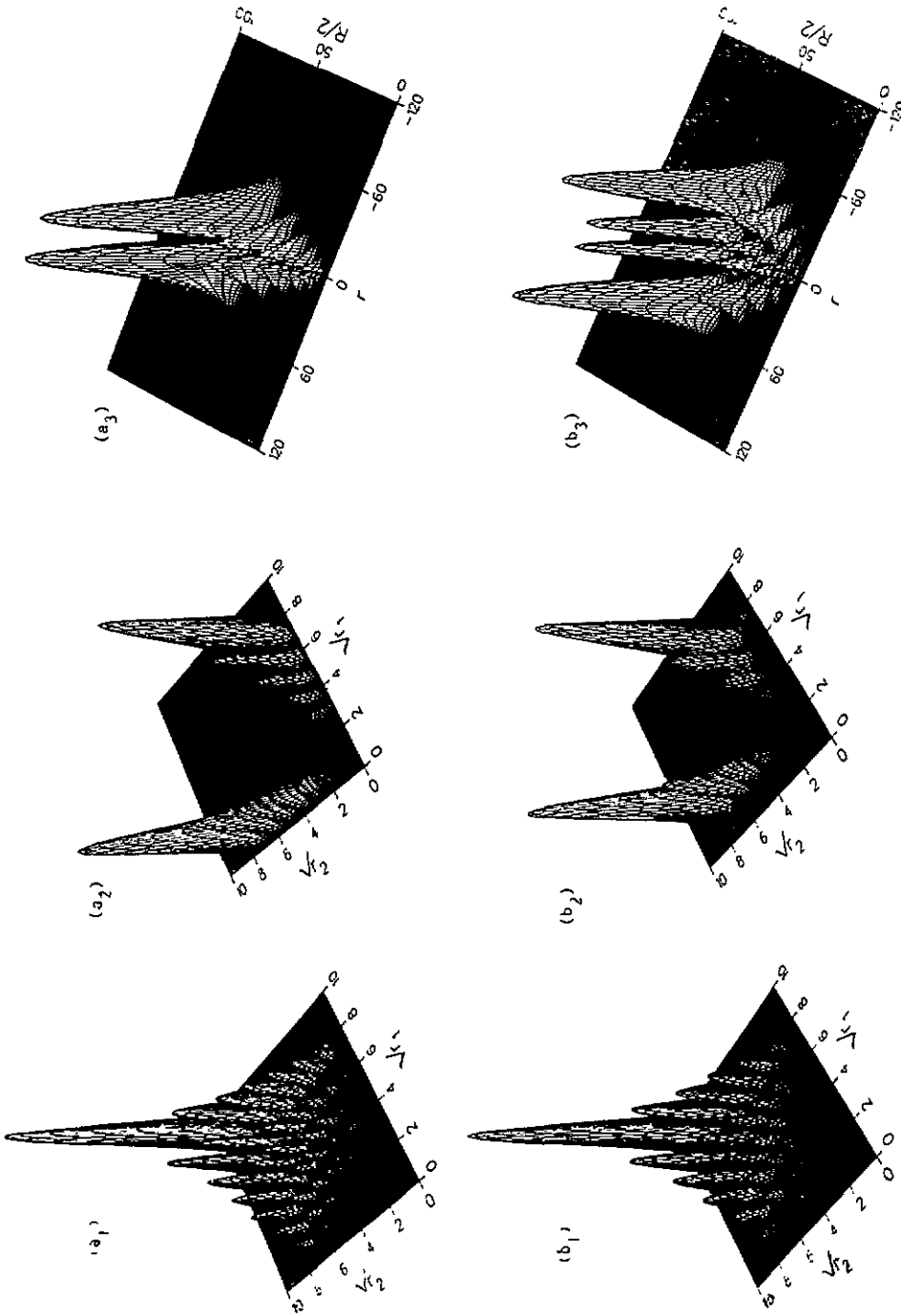


Figure 3. Conditional probability densities of ($N = n = 8$) intra-shell states for $Z = 10$ calculated by intra-shell diagonalization. The densities are plotted for fixed angle $\Theta_{12} = \pi$ (first column), $\Theta_{12} = 0$ (second column) and for $r_1 = r_2$ (third column). Note that Z -scaled coordinates are used. Probability distributions are shown for $K = 7$ (a), $K = 5$ (b), $K = -5$ (g) and $K = -7$ (h).

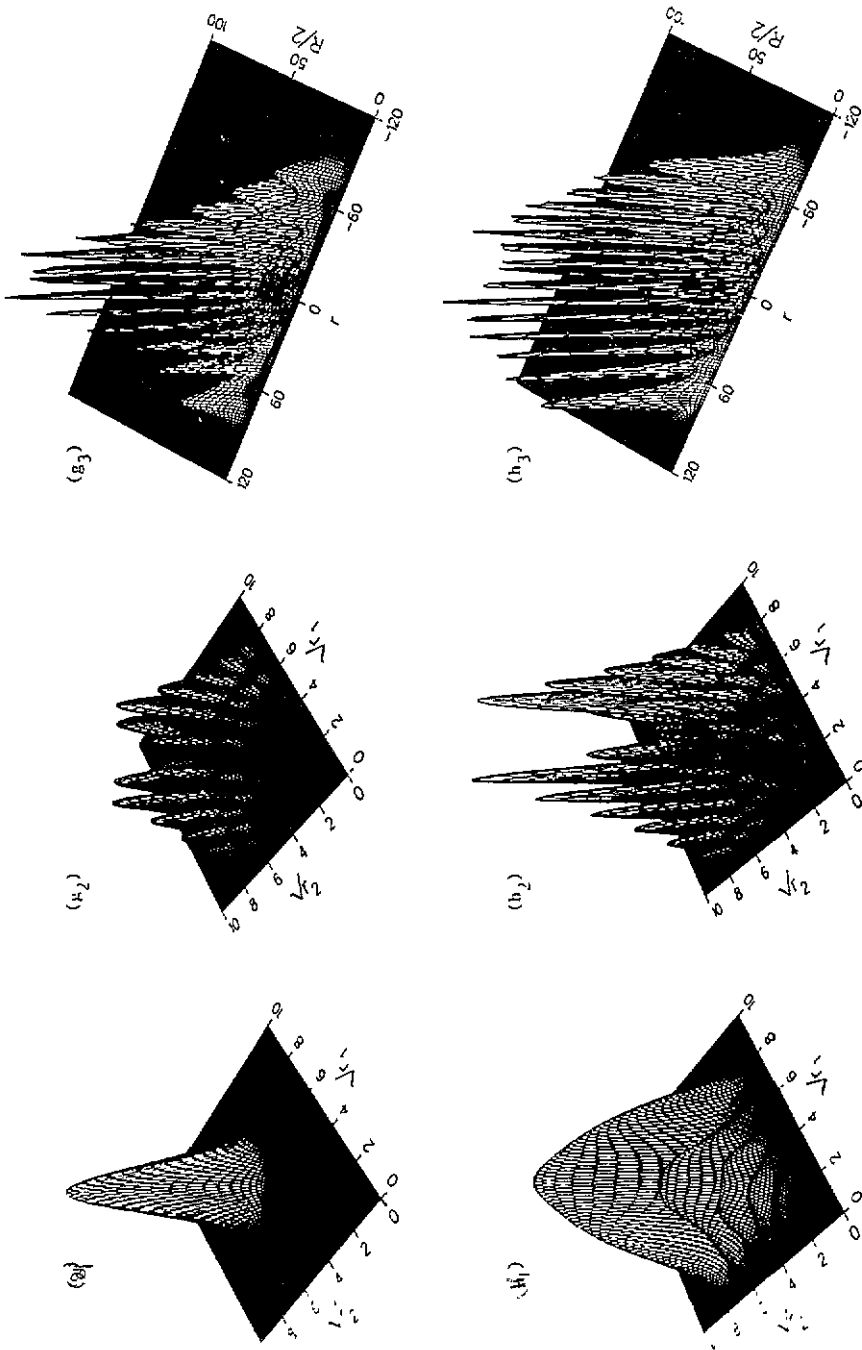


Figure 3. (Continued.)

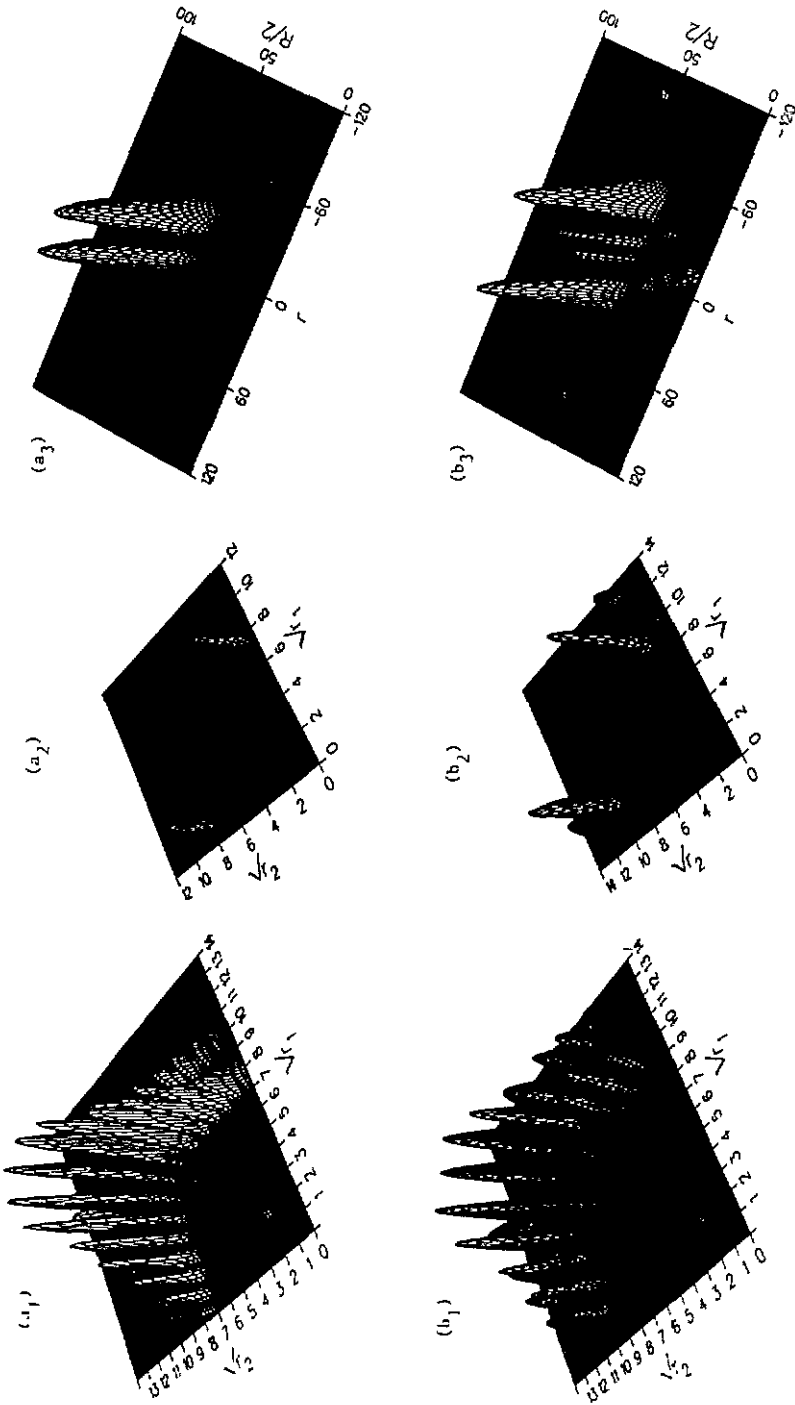


Fig. 4

Figure 4. Conditional probability densities of helium intra-shell states for $N = n = 8$ calculated by diagonalization using a near-complete basis set. The densities are plotted for fixed angle $\Theta_{12} = \pi$ (first column), $\Theta_{12} = 0$ (second column) and for $r_1 = r_2$ (third column), respectively. Probability distributions are shown for $K = 7$ (a) and $K = 5$ (b).

corresponding density obtained within the intra-shell diagonalization (figure 2(a)), the ($\Theta_{12} = \pi$) probability for $(N, K) = (8, 7)$, figure 4(a), is characterized by a strong suppression of inner maxima. Nevertheless, the dominant electron density is still located in the region at $r_1, r_2 \approx 8$ au. The particular density of the wavefunction reflects the localization along an asymmetric stretch type periodic motion of the electron pair (Ezra *et al* 1991). In contrast to the pure intra-shell character of the wavefunction shown in figure 2(a) however, the *ab initio* wavefunction contains a considerable contribution of asymmetrically excited states, dominantly from the state $N(K, T)n = 7(6, 0)9$. The $(N, K) = (8, 5)$ state exhibits similar admixtures within the ($\Theta_{12} = \pi$)-plane, see figure 4(b₁). As shown in parts (a₃) and (b₃) of the figure, the wavefunctions show $v = 0$ and $v = 1$ quanta for the bending motion, respectively. Again, this reflects the approximate separability of the bending degree of freedom from the residual internal (radial) motion.

We can in principle calculate higher lying wavefunctions $N > 8$. However, due to the high density of states and due to considerable mixing of the different Rydberg-series the wavefunctions no longer exhibit a pure intra-shell character. Thus it becomes more and more difficult to definitely relate highly doubly-excited states (large N, n) with states obtained from the intra-shell diagonalization.

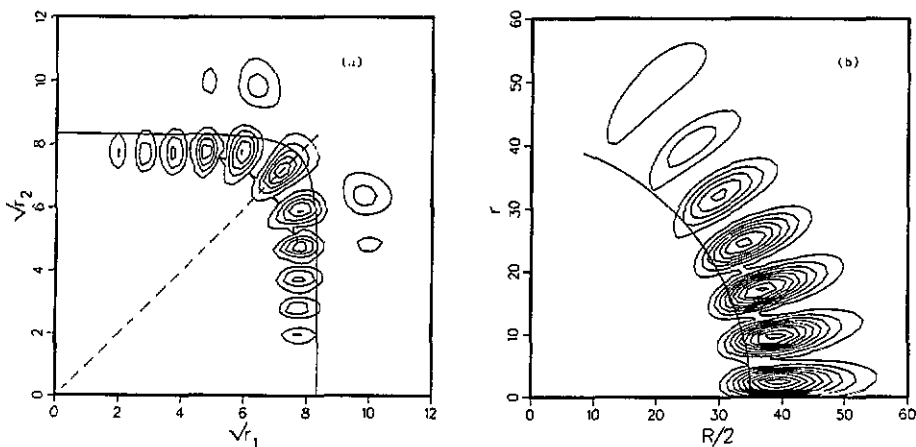


Figure 5. Contour plots of probability densities of helium intra-shell wavefunctions of minimum and maximum bending excitation and corresponding classical periodic orbits. Shown is the *ab initio* wavefunction $(N, K) = (8, 7)$ for angle Θ_{12} fixed to $\Theta_{12} = \pi$ (a) and the state $(N, K) = (7, -6)$ (from intra-shell diagonalization) for $r_1 = r_2$ (b). The asymmetric stretch orbit (full line in (a)), the Wannier orbit (broken line in (a)) and the Langmuir orbit (b) overlaid each other on the figures.

3.3. Semiclassical analysis

It is now well established that the Fourier decomposition of the spectral density relates to the periodic orbits of the corresponding classical system (Gutzwiller 1990). For the helium atom this has been demonstrated by Ezra and co-workers (Kim and Ezra 1991) for a collinear model. Furthermore, the periodic orbits are the ingredients for a semiclassical quantization of the chaotic electron pair motion in helium (Ezra *et al* 1991, Wintgen *et al* 1992). The semiclassical analysis of the intra-shell level density reveals the significance of two prominent periodic orbits, the Langmuir orbit (Langmuir 1921) and the asymmetric

stretch orbit (Richter 1991). It has been shown in Ezra *et al* (1991) that the wavefunctions of the ($K = N - 1$) states follow the collinear ($\Theta_{12} = \pi$) asymmetric stretch-type periodic orbit. Figure 5(a) shows a contour plot of the probability distribution of figure 4(a), i.e. the *ab initio* (N, K) = (8, 7) eigenstate. The asymmetric stretch-type periodic orbit is overlaid as full curve on the figure. Indeed, the quantum state is clearly localized along this fundamental mode indicating that the motion near the Wannier saddle $r_1 = r_2$ is perpendicular to the Wannier ridge $r_1 \equiv r_2$. The symmetric stretch motion (i.e. the Wannier orbit) is shown as a broken line. We have not found any states localized along the symmetric stretch. This largely verifies the conjecture expressed in Richter and Wintgen (1990a) that the symmetric stretch motion has no semiclassical significance.

For a similar correspondence between quantum states and classical periodic orbits, the states of high bending excitations should be related to the Langmuir orbit, which reflects a nearly pure bending motion of the electrons. This line of reasoning was also taken up in a recent publication by Müller *et al* (1992). Figure 5(b) shows the probability density of the (N, K) = (7, -6) state (obtained by intra-shell diagonalization!) in the Wannier-plane $r_1 \equiv r_2$ as a function of R and r . The classical Langmuir orbit is overlaid on the figure as a full line. Even though the classical orbit does not pass through the maxima of the wavefunction, the direction of quantum and classical motion appears to be very close. The expectation value $\langle \cos \Theta_{12} \rangle = 0.067$ of this state is also close to the classical average $\langle \cos \Theta_{12} \rangle_{cl} = 0.060$ along the periodic orbit. We emphasize however, that the good agreement is some kind of artefact related to the incomplete basis set used: the exact *ab initio* wavefunctions reflect a different behaviour as documented in table 1: the $\langle \cos \Theta_{12} \rangle$ expectation values for the $K = -(N - 1)$ states asymptotically ($N \rightarrow \infty$) approach the value 1, which corresponds to a collinear configuration where both electrons are mostly on the same side of the atom (Richter and Wintgen 1990b, Richter *et al* 1992). Again, this reflects the fact that for helium the upper states of the manifolds are not well represented by the intra-shell diagonalization and that asymmetric contributions to the wavefunctions are important. It is interesting to note in this context that Herrick's analytical formula (10) predicts $\langle \cos \Theta_{12} \rangle_{K=-(N-1)} = 0.5$ in the large N limit. Thus also the DESB states with $K = -(N - 1)$ cannot correspond to the Langmuir orbit for which most of the kinetic energy is located in the bending degree of freedom. However, there may be a correspondence between states of small K and an asymmetric version of Langmuir's orbit, which exists for $Z > 5$ (Richter 1991).

4. Summary

In this paper we developed a method (intra-shell diagonalization) to diagonalize the Hamiltonian of a two-electron atom in a basis of symmetrically excited electron states. The method incorporates intra-shell mixings and reproduces the correct large Z -limit of the problem, but it neglects inter-shell mixings of states of asymmetrical electron excitation. We showed that the results of the intra-shell diagonalization are of reasonable accuracy for both energies and the nodal structure of the associated wavefunctions for helium states of low bending excitation. For high lying states of the intra-shell manifolds, however, a considerable Z -dependence leads to a strong rearrangement of the electron pair wavefunctions and the corresponding states for helium are inadequately described by the large Z -limit symmetries and classification.

Acknowledgments

We would like to thank J S Briggs and J M Rost for stimulating discussions. The work was supported by the Deutsche Forschungsgemeinschaft under contract Wi877/2 and within the SFB 276 located in Freiburg.

References

- Bürgers A and Wintgen D 1993 to be published
Conneely M J and Lipsky L 1978 *J. Phys. B: At. Mol. Phys.* **11** 4135
Cooper J W, Fano U and Prats F 1963 *Phys. Rev. Lett.* **10** 518
Dmitrieva I K and Plindov G I 1988 *J. Phys. B: At. Mol. Opt. Phys.* **21** 3055
Ezra G S, Richter K, Tanner G and Wintgen D 1991 *J. Phys. B: At. Mol. Opt. Phys.* **24** L413
Fano U 1983 *Phys. Rep.* **46** 97
Feagin J M and Briggs J S 1986 *Phys. Rev. Lett.* **57** 984
— 1988 *Phys. Rev. A* **37** 4599
Frost A A, Inokuti M, and Lowe J P 1964 *J. Chem. Phys.* **41** 482
Gutzwiller 1990 *Chaos in Classical and Quantum Mechanics* (New York: Springer)
Herrick D R 1983 *Adv. Chem. Phys.* **52** 1
Herrick D R and Sinanoglu Q 1975 *Phys. Rev. A* **11** 97
Herrick D R, Kellman M E, and Polliak R D 1980 *Phys. Rev. A* **22** 1517
Ho Y K 1983 *Phys. Rep.* **99** 1
James H M and Coolidge A S 1937 *Phys. Rev.* **51** 857
Kim J H and Ezra G S 1991 *Proc. Adriatico Conf. Quantum Chaos* (Hongkong: World Scientific)
Langmuir I 1921 *Phys. Rev.* **17** 339
Lin C D 1984 *Phys. Rev. A* **29** 1019
Lin C D and Macek J 1984 *Phys. Rev. A* **29** 2317
Macek J 1968 *J. Phys. B: At. Mol. Phys.* **1** 831
Macek J and Feagin J M 1985 *J. Phys. B: At. Mol. Phys.* **18** 2161
Macias A and Riera A 1991 *Phys. Rev. A* **40** 1991
Madden R P and Codling K 1963 *Phys. Rev. Lett.* **10** 516
Müller J, Burgdörfer J and Noid D W 1992 *Phys. Rev. A* **45** 1471
Pekeris C L 1958 *Phys. Rev.* **112** 1649
Reinhardt W P 1982 *Ann. Rev. Phys. Chem.* **33** 223
Richter K 1991 *PhD thesis* University Freiburg
Richter K and Wintgen D 1990a *J. Phys. B: At. Mol. Opt. Phys.* **23** L197
— 1990b *Phys. Rev. Lett.* **65** 1965
Richter K, Briggs J S, Wintgen D and Solov'ev E A 1992 *J. Phys. B: At. Mol. Opt. Phys.* **25** 3929
Rost J M, Briggs J S and Feagin J M 1991a *Phys. Rev. Lett.* **66** 1642
Rost J M, Gersbacher R, Richter K, Briggs J S and Wintgen D 1991b *J. Phys. B: At. Mol. Opt. Phys.* **24** 2455
Wannier G H 1953 *Phys. Rev.* **90** 817
Wintgen D, Richter K, and Tanner G 1992 *Chaos* **2** 19
Wulfman C 1973 *Chem. Phys. Lett.* **23** 370
Zhen Z 1990 *Phys. Rev. A* **41** 87